Electrostatic Model of S4 Motion in Voltage-Gated Ion Channels

Harold Lecar,* H. Peter Larsson,† and Michael Grabe‡

*Department of Molecular and Cell Biology, University of California at Berkeley, Berkeley, California; †Neurological Sciences Institute, Oregon Health Sciences University, Beaverton, Oregon; and ‡Howard Hughes Medical Institute, University of California, San Francisco, California

ABSTRACT The S4 transmembrane domain of the family of voltage-gated ion channels is generally thought to be the voltage sensor, whose translocation by an applied electric field produces the gating current. Experiments on hSkMI Na^+ channels and both *Shaker* and EAG K^+ channels indicate which S4 residues cross the membrane-solution interface during activation gating. Using this structural information, we derive the steady-state properties of gating-charge transfer for wild-type and mutant *Shaker* K^+ channels. Assuming that the energetics of gating is dominated by electrostatic forces between S4 charges and countercharges on neighboring transmembrane domains, we calculate the total energy as a function of transmembrane displacement and twist of the S4 domain. The resulting electrostatic energy surface exhibits a series of deep energy minima, corresponding to the transition states of the gating process. The steady-state gating-charge distribution is then given by a Boltzmann distribution among the transition states. The resulting gating-charge distributions are compared to experimental results on wild-type and charge-neutralized mutants of the *Shaker* K^+ channel.

INTRODUCTION

S4 is a charged, membrane-spanning domain highly conserved in the superfamily of voltage-gated ion channels (reviewed by Catterall, 1988). Because it harbors 4–8 positively-charged amino acids, the S4 domain experiences intense forces in a transmembrane electric field. Thus, it is the prime candidate to be the electric-field sensor for voltage-dependent gating (Greenblatt et al., 1985; Noda et al., 1984; Guy and Seetharamulu, 1986). Field-induced translocation of the S4 charges normal to the membrane must produce a saturable charge that can be estimated for different virtual motions of S4. The motion that is most energetically favorable can be used to obtain a structurally-based prediction of the voltage-dependent gating-charge distribution (Armstrong and Bezanilla, 1973; Mannuzzu et al., 1996; reviewed by Sigworth, 1994).

A number of experimental findings suggest that the gating current is dominated by motion of the S4 charges normal to the plane of the membrane. Experiments with charge neutralizing mutations show that most, if not all, of the measured gating charge is contributed by the charged groups on the S4 domain (Aggarwal and MacKinnon, 1996; Seoh et al., 1996). Fluorescence measurements and cysteine accessibility studies suggest an outward movement of S4 groups through a membrane-solution interface. Charges enter the membrane moiety from the cytoplasmic side and exit at the extracellular side in response to depolarizing voltages (Yang and Horn, 1995; Mannuzzu et al., 1996; Yang et al., 1996; Larsson et al., 1996; Yusaf et al., 1996; Baker et al., 1998; Wang et al., 1999; Schonherr et al., 2002; Jiang et al., 2003b).

The positively-charged amino acids on transmembrane helices have been hypothesized to interact with negatively-charged amino acids on nearby helices to form ion pairs which stabilize the protein in its nonaqueous environment (Durell et al., 1998). Armstrong (1981) proposed a sliding-ratchet model whereby a highly-charged voltage sensor with a row of positive charges moves parallel to a row of negative charges in an adjacent domain thus generating a large charge separation by moving one charged notch at a time.

The 4–8 positively-charged residues of the S4 domain are thought to form a regular array at every third position of an α-helix. Because of this, Guy and Seetharamulu (1986) and Catterall (1986) suggested that S4 moves in a helical screw motion across the membrane. Intragenic suppression experiments identified negatively-charged amino acids on S2 and S3 which can interact with the positively-charged amino acids of S4 (Papazian et al., 1995; Tiwari-Woodruff et al., 1997, 2000).

For the *Shaker* K^+ channel, the voltage-dependence of the gating charge and the conductance can be modified by point mutations in which a particular S4 charge is neutralized (Papazian et al., 1991; Liman et al., 1991; Logothetis et al., 1992; Aggarwal and MacKinnon, 1996; Larsson et al., 1996; Seoh et al., 1996; Baker et al., 1998; Mannuzzu and Isacoff, 2000). We will carry out these same charge neutralizations within our electrostatic model and compare theoretical predictions with experiments. This constitutes a severe test of the model, and it elucidates the extent to which electrostatics contributes to the total free energy of voltage sensing.

Submitted May 7, 2003, and accepted for publication June 30, 2003.

Address reprint requests to Harold Lecar, Dept. of Cell and Molecular Biology, 134 LSA, MC# 3200, University of California at Berkeley, Berkeley, CA 94720. E-mail: hlecar@uclink4.berkeley.edu.

0006-3495/03/11/2854/11 $2.00

MODEL ASSUMPTIONS AND EQUATIONS

S4 movement and subunit geometry

S4 is assumed to be an α-helix. The rest of the subunit forms a caniculum (gating pore) in which S4 can undergo axial

translations. The S4 helix is also allowed to rotate around its axis. This allows for contacts to be made between S4 charges and negatively-charged residues on neighboring transmembrane domains. The rotation of S4 about its axis must be limited by the ensuing twist of extramembrane linkers which act as an effective torsional potential energy. We have ignored the torsional potential, and assumed that S4 can twist freely. Fig. 1 is a schematic diagram of assumed positions of S4 in two extreme positions; maximally retracted into the cell (Fig. 1, *A*, *C*, and *E*) and protruding into the extracellular medium (Fig. 1, *B*, *D*, and *F*). The two conformations differ by a normal displacement of 13.5 Å and a twist of 180°. Charges participating in salt bridges are labeled.

This cartoon is primarily based on structural information from three types of experiment: cysteine accessibility studies (Yang and Horn, 1995; Mannuzzu et al., 1996; Yang et al., 1996; Larsson et al., 1996; Yusaf et al., 1996; Baker et al., 1998; Wang et al., 1999; Schonherr et al., 2002), S4 charge neutralizations (Aggarwal and MacKinnon, 1996; Seoh et al., 1996), and proton transport by substituted histidines (Starace et al., 1997; Starace and Bezanilla, 2001). Another type of experiment uses pairwise neutralizations that indicate which S4 charges interact with negative amino acids in S2 and S3 (Papazian et al., 1995; Tiwari-Woodruff et al., 1997, 2000). We have restricted the placement of the negative groups in our model so that they can interact maximally with the S4 charges in the activated state (see below and Fig. 1 *B*). Specific S4 charges (R368, R371, K374, R377) were identified to be in the hydrophobic core of the protein, where they can interact with the negative groups in S2 and S3, in the activated state, but not in the deactivated state (Larsson et al., 1996; Baker et al., 1998; Tiwari-Woodruff et al., 2000). We allow a range of motion for S4 that is large enough to accommodate these results.

S4 charges are positioned every three amino acids on an ideal α-helix, and the true charge distribution is simplified to unit point charges 10 Å off of the radial axis, R_α. We assume no difference in radius for the two lysine residues and the arginine residues. The helix is erected on a fixed coordinate axis, Z. When the center point of the helix is moved to position $z \in Z$, the Z-coordinate of the i^{th} charge on S4 is denoted by $z_i(z)$, where $i = -3, -2, -1, 0, 1, 2, 3$, representing one of the seven amino acids, K380, R377, K374, R371, R368, R365, R362, respectively. An ideal α-helix has 3.6 residues per turn and a distance $a = 4.5$ Å between every third residue. The three-dimensional coordinates of the charged groups are then

$$x_i(\omega) = R_\alpha \,\mathrm{Cos}\left(\frac{5}{3}\pi \times i + \omega\right)$$

$$y_i(\omega) = R_\alpha \,\mathrm{Sin}\left(\frac{5}{3}\pi \times i + \omega\right)$$

$$z_i(z) = z + a \times i - 9, \qquad (1)$$

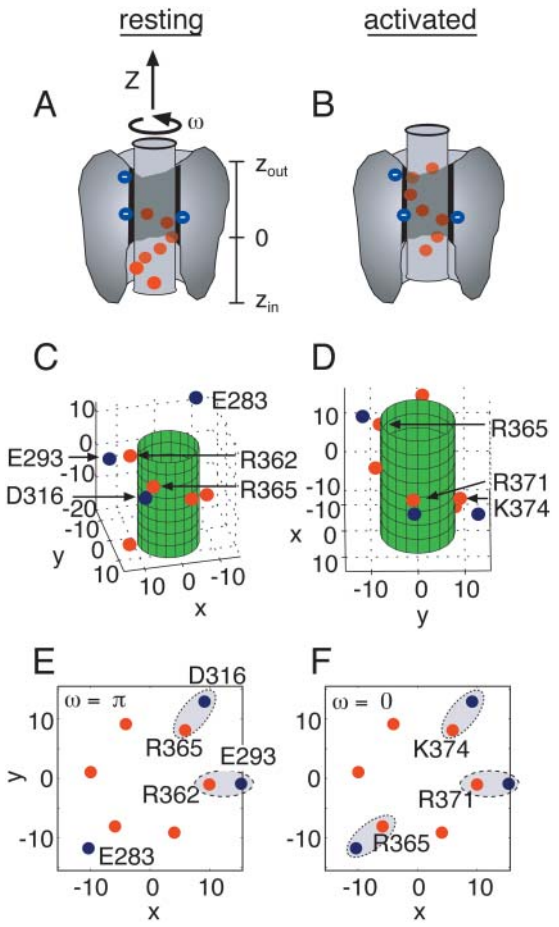

FIGURE 1 Geometry of one voltage-sensing subunit, S1–S4, in the resting (*left column*) and activated states (*right column*). Here we illustrate the fully resting state *a* and the final salt-bridge state *d* both in Fig. 2. State *e* is related to state *d* by a pure axial translation with no new salt bridges being formed. (*A*, *B*) S1–S3 is pictured as an amorphous, gray structure surrounding an α-helical S4. Acidic, negative amino acids are shown in blue and placed in proximity to the red basic residues of S4, R362–K380. The extracellular space is at the top of the molecule, and R362 is closest to this space. The region from $Z = z_{out}$ to 0 corresponds roughly to the solvent-inaccessible portion of S4 (Mannuzzu et al., 1996; Larsson et al., 1996). The length from $Z = 0$ to z_{in} corresponds to a region of S4 that is accessible to cysteine modification, but that most likely supports an electric field in the presence of a transmembrane potential. (*C*, *D*) A more precise representation of the charge geometry. Red S4 charges are pictured over a green cylinder for clarity. This cylinder is aligned along the *z*-axis, and the positive charges are placed at a radius of 10 Å. The fixed positions of the negative charges in both the resting and activated states were determined to be E283: −10.33, −11.75, and 12.6; E293: 15.28, −0.91, and 4.52; and D316: 9.13, 12.92, and 0.28. S4 charges participating in salt bridges are labeled. Key charges on S2−S3 are labeled in *C*. S4 undergoes an axial translation of 13.5 Å and a clockwise rotation of 180° (when viewed from the extracellular medium) in going from *C* to *D*. (*E*, *F*) A projection of the basic and acidic charge positions in *C* and *D* into the *x*-*y* plane. Two salt bridges are made in the resting state (indicated by *gray ellipses*), and three are made in the activated state. The positions of E283, E293, and D316 remain the same in both graphs. All lengths are in Ångstroms.

where the offset of −9 Å is introduced to place the wild-type resting state configuration close to zero. When z is zero the amino acid R365 is at $Z = 0$. Note that we have defined

a right-hand coordinate system, and that in this frame, twist motions of the helix are generally in the negative ω-direction.

Finally, the positions of the negative amino acids are not assumed a priori, but rather are determined by fitting the data as described below. However, gross features of their positions must be satisfied to be consistent with experimental evidence and obey steric constraints. The charges must fall within $Z = z_{out}$ and $Z = 0$ in Fig. 1 *A*, and they must come no closer than 2.2 Å of the S4 charges as they sweep out a 10 Å radius cylinder. We refer to the vector positions of each of these charges as **A**, **B**, and **C** for E283, E293, and D316, respectively. As we will see, our analysis arrives at charge locations which are qualitatively consistent with the work of Papazian's group (Tiwari-Woodruff et al., 1997, 2000).

Electrostatic energy of displacing S4

The electrostatic energy of the S4 helix is assumed to have three major components: 1), W_C, the Coulomb attraction among the seven positive charges on the helix and three negative charges on the neighboring S2 and S3 helices; 2), W_I, the image barrier against bringing the S4 charges from solution into the low-dielectric internal protein moiety; and 3), W_F, the work done by the applied electric field to move the S4 charges across the membrane. The total energy is the sum of these three components,

$$W(z, \omega, V) = W_C(z, \omega) + W_I(z) + W_F(z, V). \quad (2)$$

We ignored any possible motion of the negative charges, which appears to contribute no more than 10% to the gating charge. Because we are interested in *changes* in energy, we have also ignored the repulsive interactions among the S4 charges themselves. These repulsive interactions could change if the S4 helix were not rigid, or when an S4 charge passes through the protein-solution interface. The later changes will be small as long as the electric field concentrated along the S4 cylinder remains relatively constant when the helix penetrates into the high dielectric solution.

Coulomb interaction within the gating canal

We use the results of cysteine accessibility experiments, which indicate which amino acids become accessible to solution during the gating process (Larsson et al., 1996; Yusaf et al., 1996; Baker et al., 1998; Wang et al., 1999) to determine the extent of the gating canal. This region of solvent inaccessibility delimits a low-dielectric-constant moiety in which the electrostatic interactions are strongest. We take this region to extend from a point where the inner gating canal narrows, $Z = z_{in} = -14$ Å, to the outer boundary, $Z = z_{out} = 13.5$ Å. We only consider positions of S4 within this region that are consistent with accessibility studies, roughly from $z = -11$ to 6.5 Å.

The strength of the Coulomb interaction depends on the dielectric constant of the protein medium. As we discuss later, the fitting algorithm arrived at an effective dielectric constant which is typical of the protein moiety, $\varepsilon_p \sim 15$ (Cohen et al., 2002). We ignore Lorentz-field effects for close approach of the rather bulky charges, because they will be minor compared to the reorganizational effects of the local protein dipoles. In fact, continuum electrostatic models must employ a large value for the protein dielectric constant to predict the pK_a values of ionizable groups without overestimating close ion-to-ion interactions (Warshel and Papazian, 1998).

The Coulomb potential is constrained to operate only when both charges are within the low dielectric protein/membrane moiety. When, as a result of the gating motion, the charges become accessible to the electrolyte solution, the Coulomb force is shielded and decreases almost to zero. Rather than have artificially sharp boundaries, we define a shielding function which cuts off the interaction whenever a charge passes through the dielectric boundary. The effective dielectric constant across the center of the gating canal is approximated by

$$\varepsilon(z) = \varepsilon_w + \frac{1}{4}(\varepsilon_p - \varepsilon_w)\left(1 - \tanh\left(\frac{z_{in} - z}{\lambda}\right)\right) \times \left(1 - \tanh\left(\frac{z - z_{out}}{\lambda}\right)\right), \quad (3)$$

where $\varepsilon_w = 80$ is the dielectric constant of bulk water. The length constant, λ, for the smoothed boundary was 1.5 Å. The interaction energy of the S4 charges and the three neighboring negative charges is given by

$$W_C(z, \omega) = \sum_{i=-3}^{3} \sum_{j=A,B,C} \frac{q_i Q_j}{\varepsilon(z_i(z)) r_{ij}}. \quad (4)$$

Here, q_i is the charge of the i^{th} cationic group on S4. Q_j is the charge of the j^{th} negative charge on a neighboring helix (S2 or S3); and $j = A,B,C$ represent the amino acids E283, E293, and D316, respectively. The intergroup distance is given by $r_{ij}(z,\omega)$. The distances $r_{ij}(z,\omega)$ vary as the S4 domain undergoes translation and twist, and these values can be computed using Eq. 1 and the vector positions **A**, **B**, and **C**.

Image forces

The second term in Eq. 2 represents the work done by a charge as it moves toward its image across the membrane-solution interface. The image-force energy is the difference in electrostatic self-energy of a charge at a position $z_i(z)$ within the low dielectric-constant membrane and its self-energy in the electrolyte solution far from the membrane. The exact form of the self-energy for an arbitrary position within the bilayer is rather complicated (Levitt, 1975). However, the image barrier is adequately approximated by a parabola for a thin slab (<25 Å) with a large disparity in dielectric constants. Here, we use an image barrier energy with the same boundary smoothing as the effective dielectric in Eq. 3,

$$W_1(z) = \frac{1}{4}\sum_{i=-3}^{3}\frac{q_i}{2b}\left(\frac{1}{\varepsilon_p}-\frac{1}{\varepsilon_w}\right)\left(1-\tanh\left(\frac{z_{in}-z_i(z)}{\lambda}\right)\right) \times\left(1-\tanh\left(\frac{z_i(z)-z_{out}}{\lambda}\right)\right). \quad (5)$$

The symbol b is the effective radius of the arginine charge, but more generally it accounts for the effective image barrier due to all partial charges on the S4 helix being moved into solution. Best fits to the experimental data gave $b = 2.1$ Å.

Energy in applied field

The last term of Eq. 2 represents the work done by an external field in moving the S4 charges. In general, the field energy includes the work of moving the positive charges of S4 and the negative charges in the rest of the protein. We will consider only the work done by the S4 motion, given by

$$W_F(z,V) = \sum_{i=-3}^{3} q_i V f(z_i(z))$$

$$f(z) = \begin{cases} 1 & z < z_{in} \\ 1 - f_1\left(1-\dfrac{z}{|z_{in}|}\right) & z_{in} \le z < 0 \\ f_2\left(1-\dfrac{z}{|z_{out}|}\right) & 0 \le z < z_{out} \\ 0 & z > z_{out} \end{cases}, \quad (6)$$

where $f(z)$ is the profile of the electric field across the entire protein. This profile phenomenologically accounts for the small amount of the electric field, $f_1 = 15\%$, that falls off across the gating canal from $Z = z_{in}$ to 0. This is primarily due to the reduced mobility of the water in this region (Sansom et al., 1997), and the comparable size of the gating canal compared to the Debye length. The remaining portion of the field falls off across the cysteine inaccessible portion of the protein, $f_2 = 85\%$. The values for f_1 and f_2 were determined from fits to the data.

Gating charge and conductance

The total electrostatic energy, $W(z,\omega,V)$, forms an energy landscape whose value depends upon the displacement of the rigid S4 helix normal to the membrane and the twist about its axis. The energy surface displays a series of local minima corresponding to configurations with maximum Coulomb attractive energy among the seven S4 charges and the adjacent negative charges on S2 and S3. Generally, we observe five principal minima, which determine quasiequilibrium states encountered during the motion of the gating charge. If the positions of these energy wells span a simply connected path on the energy surface, then this path forms a one-dimensional reaction coordinate. The series of energy wells is skewed by the applied potential, leading to a transient change of occupancy and resultant charge displacement. The equilibrium gating charge is determined by computing the voltage-dependent changes in a Boltzmann distribution of the allowed energy states.

Energy wells that are both relatively deep, ~4–5 kT, and spatially resolvable, provide a possible structural basis for the usual transition-state models of the gating process. If the molecular geometry allows close approaches between a positive S4 charge and a negative charge in the surround, then the Coulomb energy will be dominated by the contributions from the closely approaching charge pairs. As we will see, wells generally correspond to configurations in which two or three close approaches can be made simultaneously. In such cases, one can say that the configuration is stabilized by salt bridges. In general, the Coulomb interaction is a long-range force, with next-nearest neighbors also contributing, so that the salt-bridge positions are not a priori obligatory equilibrium positions.

The positions of the energy minima are denoted by z_k^*, where k is the index of the well. When the center of S4 is at position z_k^*, the measured gating charge is equal to the external charge transferred to the membrane capacitance to neutralize the charges that have moved within the membrane. Hence, the charge for state k is given by

$$Q_k^{gate}(V) = -\frac{W(z_k^*,V) - W(z_1^*,V)}{V}, \quad (7)$$

where z_1^* is the z-position of the well corresponding to S4 in its maximally retracted position.

In the presence of an external field, the energy of state k becomes

$$w_k(V) \approx w_k(0) + Q_k^{gate}V. \quad (8)$$

For well depths greater than kT, the energy minima, w_k, can be viewed as energy levels whose relative positions change with applied potential.

Ignoring possible cooperative interactions between different S4 subunits (see Discussion), we can calculate the gating charge as a function of potential assuming a Boltzmann distribution among the energy levels of four independent subunits. The observable gating charge for one subunit is given by

$$Q(V) = \langle Q_k^{gate}\rangle \equiv \frac{\sum_k Q_k^{gate}(V)e^{-w_k(V)/kT}}{\sum_k e^{-w_k(V)/kT}}. \quad (9)$$

To be consistent with experiment, for each data set we take the most hyperpolarized membrane potential data point, V_0, as a reference for zeroing the gating-charge curve: $Q(V) \rightarrow Q(V) - Q(V_0)$. This assumes that no additional gating change movement is gained by starting at a more hyperpolarized value. We discuss this point later in the text. The present formulation of the gating charge is identical in spirit to that used by Islas and Sigworth (2001).

For comparison, we can use the same energy levels to calculate the normalized voltage-dependent conductance.

The most popular kinetic model assumes that the four gating subunits move independently to attain an activated complex, which then undergoes a voltage-insensitive concerted transition to the open state. For this model, the steady-state conductance is given by

$$G(V) \equiv \frac{G_\infty(V)}{G_{\max}} = \kappa \left[\frac{e^{-w_0(V)/kT}}{\sum_k e^{-w_k(V)/kT}} \right]^4. \qquad (10)$$

It is this normalized conductance that directly corresponds with the open probabilities, P_o, shown in the figures; we freely interchange these two variables throughout. $Q(V)$ and $G(V)$ curves are calculated by substituting the energy minima of Eq. 2 into Eqs. 9 and 10. The constant prefactor, $\kappa \cong 0.8$, is the percentage of time that a fully activated channel spends in the conducting state (corresponding to a ratio of backward-to-forward rates of 0.25). The results for the wild-type *Shaker* K^+ channel are shown in Fig. 5.

Data fitting

Gating charge vs. voltage curves were generated from the model equations and compared to experimental data recorded from the wild-type channel and charge-neutralized mutants. Each of the neutralization mutants was modeled by setting the appropriate charges, either q_i or Q_j, to zero in the energy terms. We then determined a single set of model parameters that reproduced all of the gating-charge curves simply by changing one of the two values q_i or Q_j. Best fits were determined using a Nelder-Mead search algorithm (Press, 1997). Thirteen free parameters were used, and formed into a vector: $\mathbf{p} = [\mathbf{A}, \mathbf{B}, \mathbf{C}, \varepsilon_p, b, f_1, \lambda, V_{sc}]$. Nine of these parameters are the vector positions of the negative charges, and all but the surface charge, V_{sc}, have been described above. The surface charge voltage is a shift to the experimental membrane potential, owing to the intrinsic fields that local charges impose across the protein: $V_{S4} = V + V_{sc}$, where V_{S4} is the membrane potential experienced by charges on S4, and V is the experimentally measured membrane potential.

For any given value of $\mathbf{p}$, the electrostatic potential seen by S4 was computed over the range $z = \{-11, 6.5\}$, and $\omega = \{0, 2\pi\}$. This surface was computed on a grid of 300×160 points. To increase the resolution of the minima, the vector positions of **A**, **B**, and **C** were pushed onto the closest grid points before evaluating the energy surface. Convergence testing of the best fits showed little to no deviation in the results from this step. The curvature of all points on this surface was then tested using a simple finite difference along the ω- and z-directions, and the minima were identified. These positions, z_k^* and w_k^*, and values, w_k, were stored. Each minima had to be within 20 kT of the lowest minima to be used to compute the gating charge according to Eqs. 7 and 9, but there were no other restrictions on the total number of minima. This was repeated for each of the charge mutants for the given value of $\mathbf{p}$. Once $Q(V)$ was determined for each mutant, a root-mean-square error against the appropriate experimental curve was computed. The sum of these errors was used as the fitness function in the Nelder-Mead search. The best set of parameter values was used for all calculations, and they are given in Table 1. The sensitivity of the model to changes in these parameters was also tested and reported in Table 1.

RESULTS

Wild-type electrostatic energy surface

Using Eqs. 2–6, the energy, $W(z,\omega,V)$, was computed as a function of displacement, z, and twist, ω, in absence of an external field, $V = 0$. The energy surface for the wild-type *Shaker* K^+ channel at zero-applied-potential is shown in Fig. 2 *A*. The energy landscape shows a valley running diagonally across the z,ω-plane. This is the locus of twist angles for which energy is lowest at a given displacement. The minimum-energy path is punctuated by five deeper potential wells, defining five local equilibrium states in which the charges of opposite sign are optimally paired.

This is shown more clearly in the contour plot of Fig. 2 *B*, which shows that the energy wells are approximately arranged linearly along the diagonal, except for the very last well. Thus, the S4 helix can effect a screwlike motion lurching from well to well via thermal transitions. This series of transitions constitutes a stochastic version of the helical screw motion initially proposed by Guy and Seetharamulu (1986) and Catterall (1986). In this simple calculation, we have not added torsional energy, which is expected as the linkers are twisted.

During gating, the system can undergo transitions between these dominant wells, and need not explore regions of the energy surface outside the central valley. Thus, the diagonal of the contour plot is essentially a one-dimensional reaction coordinate. Fig. 2 *C* shows the profile of energy wells

TABLE 1 Model parameters and sensitivity analysis

Parameter	Value	ΔQ_{gate} [%]	$\Delta Q_{1/2}$ [%]
z_{out}	13.5 Å	−20.8/3.4	−5.1/22.3
z_{in}	−14.0 Å	−9.9/−2.5	43.0/−30.1
b	2.12 Å	−2.6/2.1	7.0/−15.2
Position of E283	[−10.33, −11.75, 12.63] Å	0.8/−0.3	1.2/−4.3
Position of E293	[15.28, −0.92, 4.52] Å	−0.1/−0.5	3.9/−8.6
Position of D316	[9.13, 12.92, 0.28] Å	0.0/0.0	0.0/−0.8
ε_p	14.6	−0.5/0.5	2.3/−3.1
f_2	0.85	−1.3/1.3	0.0/0.0
f_1	0.15	0.2/−0.2	0.0/0.0
λ	1.47 Å	0.1/−0.2	−1.6/−1.2
V_{sc}	30.2 mV	0.0/−0.0	7.8/−7.8

Parameter values were varied ±10% and the percent change in the total gating charge, ΔQ_{gate}, and the midpoint of the gating-charge curve, $\Delta Q_{1/2}$, were recorded. Only the z-positions of the charges were varied for simplicity. For all simulations, $\varepsilon_w = 80$.

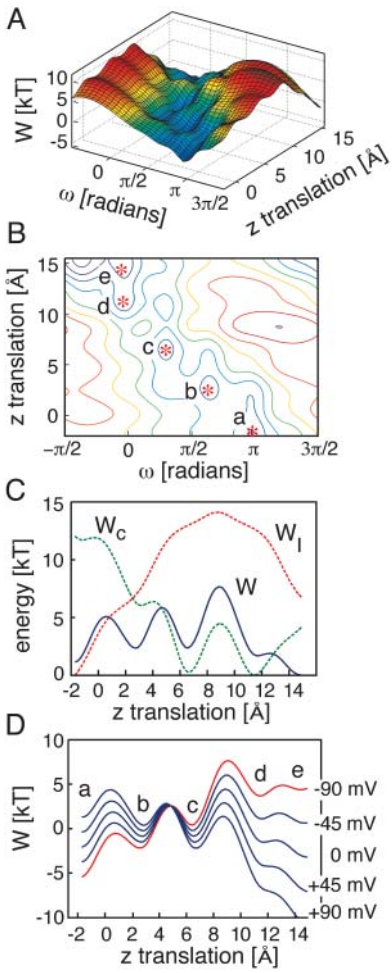

FIGURE 2 Energy landscapes of a wild-type subunit during independent translation, z, and twist, ω. (*A*) Total electrostatic energy (W) as a function of the position of S4. A clear valley is seen corresponding to the screw-helical twist motion of S4. (*B*) Energy contour plot, showing more clearly that there is a diagonal path from minimum to minimum in this energy valley. These minima are sequentially labeled *a*, *b*, *c*, *d*, and *e*. The minima *a* corresponds to the resting conformation whereas *e* corresponds to the fully activated state. Although *a*–*d* nearly fall along a diagonal path, *e* does not. (*C*) Energy barrier profile along the reaction path in *B* from states *a* to *e*. Transitions from well to well correspond to a stochastically lurching helical screw motion. The total electrostatic energy (*solid line*) is plotted along with the image force energy (*dashed red*) and the Coulomb energy (*dashed green*). (*D*) The reaction path in *C* has been drawn for several values of the membrane potential $V = -90, -45, 0, 45$, and 90 mV. The -90 mV contour is drawn in red for clarity. At hyperpolarized values, the resting state *a* is stabilized with respect to the outer states *d* and *e*. As the membrane potential depolarizes, the free energy minima shifts to the outer states, driving the translocation of the voltage sensor.

encountered along this reaction coordinate (a piecewise linear spline connects the minima in Fig. 2 *B*). We see a pattern of four energy minima, *a*–*d*, separated from each other by ~4.5 Å, followed by a final well, *e*, that is closer (~3 Å from *d*). The first four wells are largely determined by favorable salt-bridge matches between charges on S4 and neighboring acidic groups in S2–S3. The very last well, *e*, results from a pure translational displacement of S4 allowing R365 to become partially hydrated while maintaining good salt bridges with the remaining matches of state *d*. Fig. 2 *B* also shows how the energy-level pattern changes with applied potential. At large negative potentials, the resting state lies lower than the activated and intermediate states. The slopes of the different energy lines of Eq. 7 are equal to the charge Q_k^{gate}. Because the activated state has the largest charge, its energy has the steepest slope, so that the energy levels change as the external potential is increased. This accounts for the inversion of the state populations needed for voltage-dependent gating. Thus, the energy levels start off with the activated state lying highest at hyperpolarized potentials and eventually becoming the lowest at large depolarization.

Charge-neutralized mutants

Fig. 3 shows the energy wells calculated for a series of phenotypes of the *Shaker* K^+ channel studied by Seoh et al. (1996). The experiments showed different changes in gating-charge distributions as different individual charges were neutralized. The phenotypes shown are: (*A*) wild-type, ShB-IR; (*B*) E283Q; lacking the upper negative charge; (*C*) D316N, lacking the lowest negative charge; (*D*) R362Q, lacking charge $i = 3$; and (*E*) R365Q, lacking charge $i = 2$. In each of the mutant panels, the wild-type energy is shown for comparison (*dashed curve*). The cartoons on the right-hand side of the figure show how the different charge neutralizations unmake different charge matches. This has the effect of destabilizing particular energy states with respect to others. Thus, in Fig. 3 *D*, neutralization of R362 ($i = 3$) destabilized the leftmost well; state *a*, the resting state. The altered energy-well patterns are next used to predict the changes in gating-charge distribution for these mutants.

Fig. 4 shows $Q(V)$ curves calculated from Eq. 9, using the energies of Fig. 3. Additional subsidiary energy minima are used; however, this does not affect the thrust of the presentation. These theoretical curves are plotted over the experimental data of Seoh et al. (1996).

The mutants E283Q (charge *A*) and D316N (charge *C*) result from neutralization of one of the fixed negative charges. For the wild-type, wells *c*, *d*, and *e* are quite deep due to the stabilizing interactions of E283 with the upper charges in S4. Lacking these interactions in the activated state, the mutant channel requires a larger depolarization to reach these outer states, resulting in a rightward shift of the $Q(V)$ curve. The total charge moved hardly changes, because wells *a* and *e* remain the most stable states under hyperpolarized and depolarized potentials, respectively.

For mutation D316N (charge *C*), all of the wells are destabilized by the same amount, so that the energy differences have the same pattern as the wild-type. The gating charge, however, depends on the energy differences between the wells. Thus, the $Q(V)$ curve is essentially

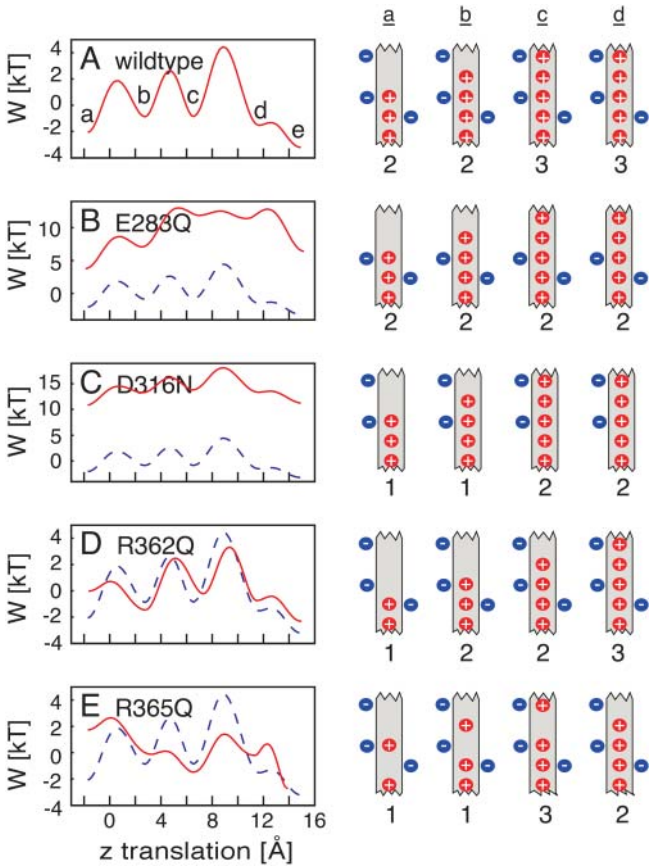

FIGURE 3 Effects of various charge neutralizations on the energy profile along the reaction path, with the right panels showing the approximate salt-bridge linkages between S4 charges and the countercharges in each of the four minima. As the position of neutralized charge is moved, different close-approach bridges are missing and the corresponding energy states are destabilized. (*A*) Wild-type ShB-IR channels. (*B*) Neutralization of the negative charge E283Q destabilizes the outer wells with respect to the inner wells *a* and *b*. In general the electrostatic energy of the system is greatly elevated upon charge neutralization of the negative charges. (*C*) D316N is the most severe charge neutralization in terms of overall energetics; however, the relative number of salt contacts made in each of the states is invariant, resulting in an energy profile that is similar to wild-type. (*D*) The most extracellular S4 charge, R362Q, is neutralized, and the deactivated state is destabilized. (*E*) R365Q is neutralized, stabilizing the middle states *b* and *c* with respect to the resting and activated states. This gives rise to the anomalous voltage-dependence in the gating charge *Q* seen in Fig. 4 *E*. The dashed curve in each panel is the wild-type energy, shown for comparison.

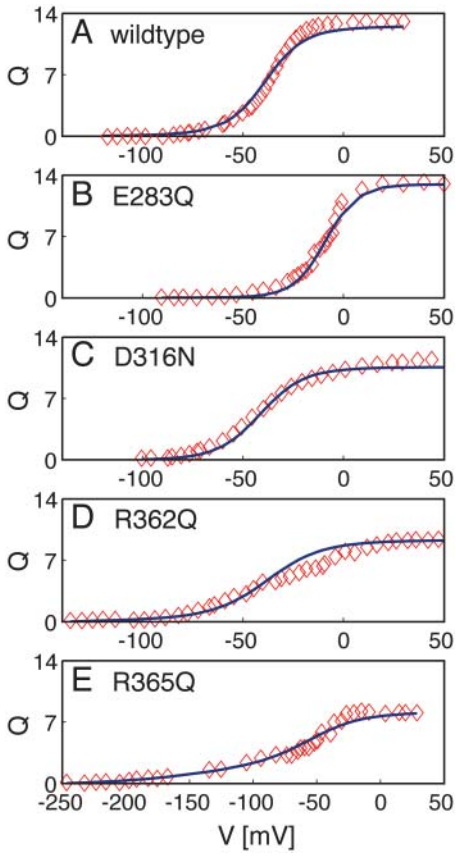

FIGURE 4 Voltage-dependence of gating for wild-type and mutant channels. Comparison with experimental data of Seoh et al. (1996) (*diamonds*) and theory (*solid line*). For each channel we show gating-charge displacement, *Q*, as a function of voltage, *V*. Experimental data for *Q* were taken directly from Seoh et al. (1996) using the program Data Thief II (Bas Tummers, Eindhoven, The Netherlands). (*A*) Wild-type ShB-IR channels, (*B*) E283Q neutralized, (*C*) D316N neutralized, (*D*) R362Q neutralized, and (*E*) R365Q neutralized. Fits to the data were performed as explained in the text, and all parameters are featured in Table 1. The original data for mutant R362Q was normalized to unity due to an inability to calibrate the currents. Here we have scaled the original data by a factor of 9.3 to compare with results from the model.

unshifted. For this mutant, wells *d* and *e* are nearly equal, so that the distance-weighted charge movement has shifted to a slightly smaller value, giving a somewhat smaller total gating charge and concomitantly less-steep slope.

When the topmost charge, R362 ($i = 3$), is neutralized, the strong interaction with D316 is missing in the resting state, leading to its destabilization (Fig. 4 *D*). Since the destabilized state, *a*, is unoccupied at the ordinary resting potential, the gating transition essentially occurs from *b* to *e*, thus carrying less gating charge and consequently exhibiting a less steep slope. In the intermediate and activated configurations, the neutralized charge is remote from any of the negative charges, so that the overall energy is unaffected.

Neutralization of R365 ($i = 2$) destabilizes the two leftmost wells, as shown in Fig. 3 *E*, resulting in the breakup of the gating curve into two components and a broad spread of the gating curve over an extended voltage region, as can be seen from Fig. 4 *E*.

It is interesting to compare mutant R365Q to mutant R362Q. For both mutations, well *a* is destabilized, since the resting state involves a simultaneous match of the two topmost S4 charges, and each of these mutants negates one of the matches. However, mutant R362Q recaptures the double match by moving up one notch, whereas mutant R365Q is still destabilized after moving up, so that both wells *a* and *b* are destabilized for R365Q. Furthermore, the intermediate state *c* is stabilized and the active state *d* is

destabilized for R365Q relative to R362Q, because of the different positions of the neutralized charge. Thus, of all the mutants, R365Q is the only one for which three out of the four states are altered. This has the effect of separating the $Q(V)$ curve into several components, so that it is spread over a much larger voltage range than any other case, as is shown (both theoretically and experimentally) in Fig. 4 *E*.

Fig. 5 shows a detailed comparison between the wild-type and R365Q. The energy contour plot of the wild-type, shown in Fig. 5 *A*, has a string of energy minima cutting diagonally across the displacement/twist plane. This diagonal corresponds roughly to a helical twist path having the periodicity of the S4 charges. Thus, successive energy minima are reached by twisting the S4 helix 60° in the opposite sense to the α-helical angle. In this case, the reaction path from well to well can be thought of as a lurching helical screw motion. For the mutant R365Q, shown in Fig. 5 *B*, the first stable state at $z = -2$ has been displaced by $\sim -120°$. Because of the missing charge at R365, the most stable resting position cannot be the usual double salt-bridge configuration, but rather one in which the top charge is shared by the two negative charges (E283 and D316). Now the charges are situated in such a fashion that the next two equilibrium points, *b* and *c*, can be reached by a pure translation. Thus, the first part of the reaction path does not approximate a screw motion, but rather a 9 Å vertical translocation through three more-or-less equally deep minima.

Fig. 5, *C* and *D*, show the probabilities of occupying the various states as a function of membrane potential (calculated from Eq. 9). For the wild-type, the intermediate states, *b* and *d*, are never occupied >10% of the time, so that gating charge is close to a two-state system (Fig. 4 *A*). For R365Q, Fig. 5 *D* shows that the intermediate states, *b* and *c*, have large occupancies. In fact, they dominate over a wide voltage range. Thus, the gating charge moves through resolvable intermediate states, and the charging curves are spread over a broad voltage, nearly twice that of the wild-type and other mutants (Fig. 4 *E*).

Fig. 5, *E* and *F*, show the voltage-dependent conductances calculated from Eq. 10, with no change of parameters. We see that the wild-type is in agreement with experiment, but R365Q is shifted by ~10 mV in the depolarizing direction. In both cases, the experimental curves are slightly steeper than those calculated. These results depend on the kinetic model used for the conductance. Since Eq. 10 is somewhat of an oversimplification, neglecting such features as cooperativity between subunits and the small voltage-dependence of the concerted transitions, the agreement is satisfactory.

DISCUSSION

These calculations show that a simple electrostatic model can give a qualitative account of the gating charge for both wild-type and mutant *Shaker* K^+ channels. For this type of model to be useful, the electrostatic energy profile must exhibit well-resolved energy wells. Since these energy minima must emerge from the superposition of a number of long-range interactions, the discrete minima are not manifest in an arbitrary distribution of charges on S4. Charges spaced too far apart will not give sufficient gating current for a feasible

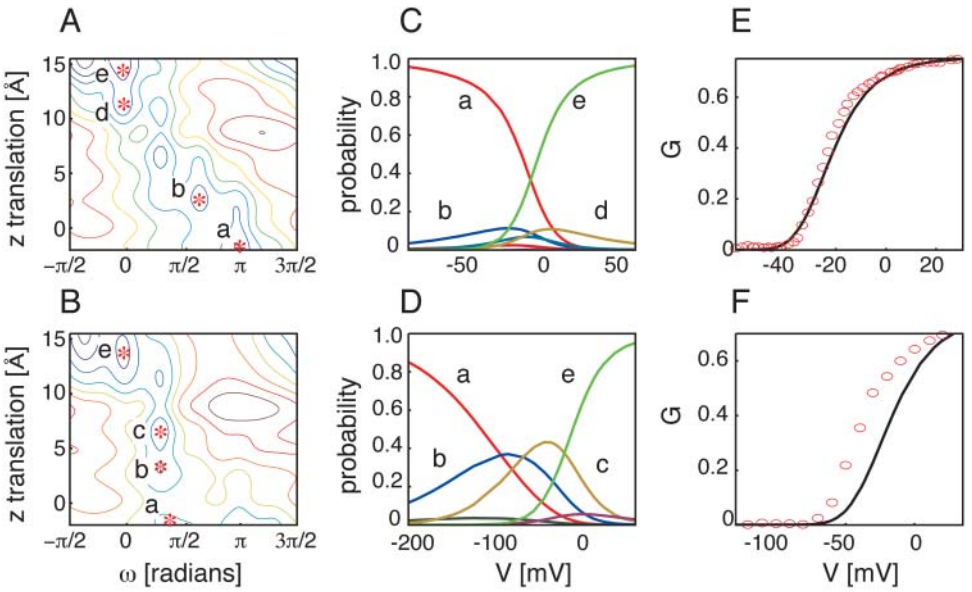

FIGURE 5 Reaction paths, state-dependent probabilities, and conductances for wild-type (*top panels*) and R365Q channels (*bottom panels*). (*A*, *B*) Contour plots of the total electrostatic energy with the four most significant wells labeled (*red asterisk*). Note that the reaction path for R365Q is nearly a pure axial translation with little rotation about the S4 axis. (*C*, *D*) State-dependent probabilities corresponding to the energy minima in the contour maps in *A* and *B*. Wild-type channels are nearly a pure two-state system between wells *a* and *e*. Subsidiary states reach no higher than 10% occupancy. Meanwhile, states *b* and *c* are significantly populated, at ~40%, for the mutant R365Q. Moreover, even at very hyperpolarized potentials, state *a* is only at 80% occupancy. (*E*, *F*) Conductance from state-dependent probabilities. The experimental data of Seoh et al. (1996) (*circles*) is compared with theory (*solid line*). Experimental data for the open probabilities, P_o, were taken directly from Seoh et al. (1996) using Data Thief II. The theory curves were generated using Eq. 10, with a value of $\kappa = 0.76$. When S4 was in state *d* or *e* it was assumed that the concerted transition could occur; therefore, the sum of the probabilities of being in states *d* and *e* were raised to the fourth power in Eq. 10. There is little deviation in the shapes of the $G(V)$ curves if the concerted transitions can only occur from state *e*. Note that $G(V)$ curves were not fit to the model; the excellent agreement between theory and experiment is a direct consequence of first fitting the gating-charge data and then assuming subunit cooperativity is required for channel opening.

motion; charges spaced too closely will not give resolvable minima when the S4 segment is moved. Therefore, this analysis works best if S4 forms an α-helix.

The observed gating charge is quite large, 12–13 electronic charges for the wild-type, which means that each S4 helix must carry the equivalent of 3.2 charges across the full transmembrane potential. One way to achieve such a large charge translocation is for S4 to move a relatively large normal distance through the gating canal and for the bulk of the voltage drop to be across this low-dielectric constant region. In our particular model, no single charge actually does this; however, the upper charges cross the majority of the field. It is conceivable that a thin gating canal separating cytoplasmic and extracellular spaces could give rise to a large gating charge with a very small motion of S4 (Asamoah et al., 2003). This involves a local environment that we have not yet explored. Working with relatively well-packed models of *Shaker* using Poisson-Boltzmann solvers, we find that the electrostatic profile across the sensor is smoothly varying even in the presence of water-filled crevices modeled as bulk (data not shown). Therefore, we favor large motions of S4 to describe the gating charge rather than small ones. This requires the S3–S4 and S4–S5 linker regions to be quite flexible, but this seems to agree with the recent crystallographic work of MacKinnon's group on a related voltage-gated potassium channel from *Aeropyrum pernix*. They solved the voltage-sensor domain, S1–S4, both in isolation and in the presence of the entire channel, and they found that the secondary elements S2, S3, and S4 retained all of their α-helical nature despite being extended in the full-length structure (Jiang et al., 2003a). Moreover, in a followup study using biotin-avidin tethering in reconstituted bilayers, they determined that the center of mass of the voltage sensor undergoes a large 20 Å movement normal to the membrane (Jiang et al., 2003b). From this they concluded an alternative reaction path involving the motion of the S4–S3b ''voltage paddle'' predominantly through the lipid membrane (Jiang et al., 2003a,b). The relationship between this new work and the body of existing data is still unclear (Cohen et al., 2003), but this could have important consequences on the energetics of activation gating.

As the voltage sensor moves, we believe that different parts of the protein must come into close contact with each other at different times. This makes it possible for multiple electrostatic energy wells to emerge along the activation pathway, which seems to be essential for explaining the R365Q charge mutant (Seoh et al., 1996). Our calculations suggest that favorable electrostatic matches are made nearly simultaneously between two consecutive S4 amino acids toward the cytoplasmic domain and a third S4 charge close to the extracellular surface. In the resting state these pairs are E293–R362 and D316–R365 (the outer one missing), whereas the activated state involves E283–R365, E293–R371, and D316–K374 (see Fig. 1). This corresponds to a 15–16 Å movement of the S4 helix relative to the rest of the protein. Our results indicate that the wild-type curves are robust for small changes in many of the structural and energetic parameters when a large spacing exists between the negative charge, E283, near the outer surface of the membrane, and the pair, E293 and D316, at the cytoplasmic mouth of the gating pore (see Table 1). The system is most sensitive to the protein boundaries because the solvation energy of the S4 charges plays a key role in the inner and outer wells. However, for all of the variations carried out in the sensitivity analysis, the two-state characteristic of the wild-type curve was not affected.

Both Silverman et al. (2003) and Durell et al. (1998) have used molecular approaches to understand the packing geometry of voltage-gated potassium channels in both their resting and activated states. The construction of both of these models takes into account a wealth of experimental information. Additionally, Durell et al. (1998) use sequence homology analysis to better understand helix packing and the propensity for nonideal structural units. On the other hand, Silverman et al. (2003) employ a rigorous simulated annealing algorithm that simultaneously addresses most experimental restraints (see article by Roux, 2002). However, these models predict that charged groups on S2–S3 encounter three different S4 amino acids during activation gating, whereas the reaction path in Fig. 3 *A* has four close approaches. With a smaller relative motion between components, it is hard to imagine that they will produce enough gating current to describe the experimental data.

Where did all the gating charge go? The charge neutralization of a single residue can sometimes reduce the gating charge by as much as seven electron charges (Seoh et al., 1996). At most we expect the gating charge to be reduced by four charges if the mutated amino acid crosses the entire transmembrane field. Mutant R365Q has a reduction of 5.0 charges, whereas R362Q is reduced by 3.8. In our model, no single residue crosses the entire transmembrane field, so a reduction as large as 3.8 charges seems implausible, let alone 5.0. There are two reasons why this happens. First, the energy-minima shift slightly for any given mutation, and this can result in less charge displacement in the external field as S4 moves from the innermost well to the activated state. More importantly, the practical definition of the macroscopic gating current involves zeroing the gating current at the most hyperpolarized potential to be consistent with the experimental measurements (see discussion of Eq. 9). In Fig. 5 *D* we see that the innermost well, state *a*, has an 85% occupancy at -200 mV, whereas the wild-type occupancy of this state is nearly 100% at -120 mV. Consequently, even though the experimental curve appears to have reached a horizontal asymptote, more gating charge can be measured by starting at a more hyperpolarized membrane potential. This corresponds to preparing an initial system with a higher percentage of the S4 subunits in the most retracted position, which results in more charge transfer at any given membrane potential. We believe that this

explains the missing components of the charge for mutants R368N and R371Q. For example, our calculations predict that R362Q is equally populating states *a* and *b* at the most hyperpolarized recordings. Since state *b* is more stable than state *a*, the gating charge transiently plateaus at −120 mV despite the existence of a charge transfer component to the left of this value.

There are several charge mutants, just mentioned, that we have not quantitatively fit: R371Q, R368N, and E293Q. Qualitatively these mutations can be understood with the model, but the absolute shift of the *Q-V* curves along the voltage axis could not be simultaneously fit among all mutant curves with one set of parameters. This is not surprising because, in general, electrostatics is not the only factor contributing to the free energy of voltage gating. Conservative substitutions of hydrophobic residues in S4 have been shown to dramatically shift the activation curve along the voltage axis (Lopez et al., 1991). Gating mutations lacking overt electrostatic components, such as these, or that seriously disrupt channel structure, cannot be understood with the current simple model. It is at this point that a more precise model such as those constructed by Bob Guy or Benoit Roux would be required.

For different assumptions about the molecular geometry, the energy topography may exhibit subsidiary hills and valleys. These subsidiary minima do not affect the fit to equilibrium properties of gating but are bound to make more of a difference if the model were used to make kinetic predictions. For example, it is not clear how closely a Fokker-Planck description of random migration through the energy landscape would coincide with a transition-state model of hopping between the major energy wells. The former might, for example, predict high-frequency gating fluctuations which are not inherent in a discrete-state model. On the other hand, a smoothed energy landscape, with only the deep wells taken into account, leads to a transition-state kinetic scheme which can be compared to the prevailing empirical schemes for channel activation (Zagotta et al., 1994; Schoppa and Sigworth, 1998).

Finally, although there are many free parameters used to fit the model to the data, there is a surprising correspondence between the final values and measured quantities. As mentioned, the effective protein dielectric constant is close to values recently measured in protein G (Cohen et al., 2002). With this value and reasonable considerations for the closeness of salt bridges, the binding energies for buried, charged amino acids are in accord with more molecular calculations based on proteins of known crystal structures (Kumar and Nussinov, 1999). The local protein environment and external field profile across S4 is similar to that proposed by Islas and Sigworth in their study of ionic strength effects on gating charge. The positions of negative charges E283, E293, and D316 are reasonably consistent with those presented by Papazian's group in collaboration with Roux; however, they are not identical (Silverman et al., 2003). Lastly, a surface charge value of $V_{sc} \sim 30$ mV gave rise to the best fits among all data sets. Measurements of the surface potential in *Shaker* K^+ channels range from 20 to 45 mV (Elinder et al., 1998; Asamoah et al., 2003).

CONCLUSION

We have attempted to understand the rearrangements of the voltage sensor that take place during activation gating by considering the gating-charge movement that is concomitant with this step. This consideration places constraints upon the motion and local environment of the voltage sensor, and it can be used to rule out molecular motions. As a first step, we have adopted a very simplified approach to the geometry and electrostatics that, when coupled with the proper statistical considerations, encompasses the salient features of voltage-sensing and gating-charge movement. We have worked this model out within the context of the traditional, yet varied, view of the voltage sensor (for reviews see Gandhi and Isacoff, 2002; Bezanilla, 2002). We believe that many of the elements considered here, such as solvation of S4, the making and breaking of electrostatic pairs, and the transmembrane potential profile, will prove to be key features as more sophisticated models are developed.

M.G. is indebted to Lily Jan (Howard Hughes Medical Institute, University of California at San Francisco) both for stimulating discussions and financial support. We thank Ehud Isacoff (University of California at Berkeley), Medha Pathak (University of California at Berkeley), Fredrik Elinder (Karolinska Institutet), Smita Nayak (Stanford University), Helen Lai (University of California at San Francisco), and Alex Fay (University of California at San Francisco) for comments on the manuscript.

This study was supported by National Institutes of Health grant NS043259 to H.P.L.; and M.G. is a Howard Hughes Medical Institute Computational Fellow.

REFERENCES

Aggarwal, S. K., and R. MacKinnon. 1996. Contribution of the S4 segment to gating charge in the *Shaker* K^+ channel. *Neuron.* 16:1169–1177.

Armstrong, C. M., and F. Bezanilla. 1973. Currents related to movement of gating particles of sodium channels. *Nature.* 242:459–461.

Armstrong, C. M. 1981. Sodium channels and gating currents. *Physiol. Rev.* 61:644–683.

Asamoah, O. K., J. P. Wuskell, L. M. Leow, and F. Bezanilla. 2003. A fluorometric approach to local electric field measurements in a voltage-gated ion channel. *Neuron.* 37:85–97.

Baker, O. S., H. P. Larsson, L. M. Mannuzzu, and E. Y. Isacoff. 1998. Three transmembrane conformations and sequence-dependent displacement of the S4 domain in *Shaker* K^+ channel gating. *Neuron.* 20:1283–1294.

Bezanilla, F. 2002. Voltage sensor movements. *J. Gen. Physiol.* 120:465–473.

Catterall, W. A. 1988. Structure and function of voltage-sensitive ion channels. *Science.* 242:50–61.

Catterall, W. A. 1986. Molecular properties of voltage-sensitive sodium channels. *Annu. Rev. Biochem.* 55:953–985.

Cohen, B. E., T. B. McAnaney, E. S. Park, Y. N. Jan, S. G. Boxer, and L. Y. Jan. 2002. Probing protein electrostatics with a synthetic fluorescent amino acid. *Science*. 296:1700–1703.

Cohen, B. E., M. Grabe, and L. Y. Jan. 2003. Answers and questions from the KvAP structures. *Neuron*. 39:395–400.

Durell, S. R., Y. Hao, and H. R. Guy. 1998. Structural models of the transmembrane region of voltage-gated and other K^+ channels in open, closed, and inactivated conformations. *J. Struct. Biol*. 121:263–284.

Elinder, F., Y. Liu, and P. Arhem. 1998. Divalent cation effects on the *Shaker* K channel suggest a pentapeptide sequence as determinant of functional surface charge density. *J. Membr. Biol*. 165:183–189.

Gandhi, C. S., and E. Y. Isacoff. 2002. Molecular models of voltage sensing. *J. Gen. Physiol*. 120:455–463.

Greenblatt, R. E., Y. Blatt, and M. Montal. 1985. The structure of the voltage-sensitive sodium-channel–inferences derived from computer-aided analysis of the electrophorus-electricus channel primary structure. *FEBS Lett*. 193:125–134.

Guy, H. R., and P. Seetharamulu. 1986. Molecular model of the action potential sodium channel. *Proc. Natl. Acad. Sci. USA*. 83:508–512.

Islas, L. D., and F. J. Sigworth. 2001. Electrostatics and the gating pore of *Shaker* potassium channels. *J. Gen. Physiol*. 117:69–89.

Jiang, Y., A. Lee, J. Chen, V. Ruta, M. Cadene, B. T. Chait, and R. MacKinnon. 2003a. X-ray structure of a voltage-dependent K^+ channel. *Nature*. 423:33–41.

Jiang, Y., V. Ruta, J. Chen, A. Lee, and R. MacKinnon. 2003b. The principle of gating charge movement in a voltage-dependent K^+ channel. *Nature*. 423:42–48.

Kumar, S., and R. Nussinov. 1999. Salt bridge stability in monomeric proteins. *J. Mol. Biol*. 293:1241–1255.

Larsson, H. P., O. S. Baker, D. S. Dhillon, and E. Y. Isacoff. 1996. Transmembrane movement of the *Shaker* K^+ channel S4. *Neuron*. 16:387–397.

Levitt, D. G. 1975. General continuum analysis of transport through pores. 1. Proof of Onsager's reciprocity postulate for uniform pore. *Biophys. J*. 15:533–551.

Liman, E. R., P. Hess, F. Weaver, and G. Koren. 1991. Voltage-sensing residues in the S4 region of a mammalian K^+ channel. *Nature*. 353:752–756.

Logothetis, D. E., S. Movahedi, C. Satler, K. Lindpaintner, and B. Nadalginard. 1992. Incremental reductions of positive charge within the S4 region of a voltage-gated K^+ channel result in corresponding decreases in gating charge. *Neuron*. 8:531–540.

Lopez, G. A., Y. N. Jan, and L. Y. Jan. 1991. Hydrophobic substitution mutations in the S4 sequence alter voltage-dependent gating in *Shaker* K^+ channels. *Neuron*. 7:327–336.

Mannuzzu, L. M., and E. Y. Isacoff. 2000. Independence and cooperativity in rearrangements of a potassium channel voltage sensor revealed by single subunit fluorescence. *J. Gen. Physiol*. 115:257–268.

Mannuzzu, L. M., M. M. Moronne, and E. Y. Isacoff. 1996. Direct physical measure of conformational rearrangement underlying potassium channel gating. *Science*. 271:213–216.

Noda, M., S. Shimizu, T. Tanabe, T. Takai, T. Kayano, T. Ikeda, H. Takahashi, H. Nakayama, Y. Kanaoka, N. Minimino, K. Kangawa, H. Matsuo, M. A. Raftery, T. Hirose, S. Inayama, H. Hayashida, T. Miyata, and S. Numa. 1984. Primary structure of *Electrophorus electricus* sodium-channel deduced from cDNA sequence. *Nature*. 312:121–127.

Papazian, D. M., X. M. Shao, S. A. Seoh, A. F. Mock, Y. Huang, and D. H. Wainstock. 1995. Electrostatic interactions of S4 voltage sensor in *Shaker* K^+ channel. *Neuron*. 6:1293–1301.

Papazian, D. M., L. C. Timpe, Y. N. Jan, and L. Y. Jan. 1991. Alteration of voltage-dependence of *Shaker* potassium channel by mutations in the S4-sequence. *Nature*. 349:305–310.

Press. W.H. 1997. Numerical Recipes in C: The Art of Scientific Computing. 2nd Ed. Cambridge University Press, New York, NY.

Roux, B. 2002. What can be deduced about the structure of *Shaker* from available data? *Novart. Fdn. Symp*. 245:84–108.

Sansom, M. S., G. R. Smith, C. Adcock, and P. C. Biggin. 1997. The dielectric properties of water within model transbilayer pores. *Biophys. J*. 73:2404–2415.

Schonherr, R., L. M. Mannuzzu, E. Y. Isacoff, and S. H. Heinemann. 2002. Conformational switch between slow and fast gating modes: allosteric regulation of voltage sensor mobility in the EAG K^+ channel. *Neuron*. 35:935–949.

Schoppa, N. E., and F. J. Sigworth. 1998. Activation of *Shaker* potassium channels. III. An activation gating model for wild-type and V2 mutant channels. *J. Gen. Physiol*. 111:313–342.

Seoh, S. A., D. Sigg, D. M. Papazian, and F. Bezanilla. 1996. Voltage-sensing residues in the S2 and S4 segments of the *Shaker* K^+ channel. *Neuron*. 16:1159–1167.

Sigworth, F. J. 1994. Voltage gating of ion channels. *Quart. Rev. Biophys*. 27:1–40.

Silverman, W. R., B. Roux, and D. M. Papazian. 2003. Structural basis of two-stage voltage-dependent activation in K^+ channels. *Proc. Natl. Acad. Sci. USA*. 100:2935–2940.

Starace, D. M., and F. Bezanilla. 2001. Histidine scanning mutagenesis of basic residues of the S4 segment of the *Shaker* K^+ channel. *J. Gen. Physiol*. 117:469–490.

Starace, D. M., E. Stefani, and F. Bezanilla. 1997. Voltage-dependent proton transport by the voltage sensor of the *Shaker* K+ channel. *Neuron*. 19:1319–1327.

Tiwari-Woodruff, S. K., M. A. Lin, C. T. Schulteis, and D. M. Papazian. 2000. Voltage-dependent structural interactions in the *Shaker* K^+ channel. *J. Gen. Physiol*. 115:123–138.

Tiwari-Woodruff, S. K., C. T. Schulteis, A. F. Mock, and D. M. Papazian. 1997. Electrostatic interactions between transmembrane segments mediate folding of *Shaker* K^+ channel subunits. *Biophys. J*. 72:1489–1500.

Warshel, A., and A. Papazian. 1998. Electrostatic effects in macromolecules: fundamental concepts and practical modeling. *Curr. Opin. Struct. Bio*. 8:211–217.

Yang, N., A. L. George, Jr., and R. Horn. 1996. Molecular basis of charge movement in voltage-gated sodium channels. *Neuron*. 16:113–122.

Yang, N., and R. Horn. 1995. Evidence for voltage-dependent S4 movement in sodium channels. *Neuron*. 15:213–218.

Yusaf, S. P., D. Wray, and A. Sivaprasadarao. 1996. Measurement of the movement of the S4 segment during the activation of a voltage-gated potassium channel. *Pflugers Arch*. 433:91–97.

Wang, M. H., S. P. Yusaf, D. J. Elliott, D. Wray, and A. Sivaprasadarao. 1999. Effect of cysteine substitutions on the topology of the S4 segment of the *Shaker* potassium channel: implications for molecular models of gating. *J. Physiol*. 521:315–326.

Zagotta, W. N., T. Hoshi, and R. W. Aldrich. 1994. *Shaker* potassium channel gating. III. Evaluation of kinetic models for activation. *J. Gen. Physiol*. 103:321–362.